INTERNATIONAL JOURNAL FOR NUMERICAL METHODS IN FLUIDS
Int. J. Numer. Meth. Fluids 2002; **40**:241–251 (DOI: 10.1002/fld.335)

A shape function approach for high- and low- Reynolds near-wall turbulence models

V. Boyer[1,*,†] and D. Laurence[2]

[1] *E.D.F., M.F.T.T., 6 quai Watier, BP 49, 78400 Chatou Cedex, France*
[2] *U.M.I.S.T., Department of Mechanical Engineering, P.O. Box 88, Manchester, M60 1QD, U.K.*

SUMMARY

A new numerical approach for wall functions is proposed, in order to bridge the gap between low- and high-Reynolds near-wall turbulence modelling. It allows arbitrary sizes of near-wall cells with the objective of using local grid refinement or adaptive meshes in industrial calculations. This finite volume-finite element approach is based on the introduction of assumed shape functions into the energy conservation equations, for the determination of four wall scalings factors. Equilibrium assumptions are avoided, and replaced by formal integration of budget equations in the first cell. The approach is proved accurate and stable in a simple channel flow, but the formalism was developed for non-equilibrium situations where it still needs to be tested. Copyright © 2002 John Wiley & Sons, Ltd.

KEY WORDS: shape function; wall function; finite volume-finite element method; arbitrary near-wall cell size; energy conservation

1. OBJECTIVES

The most widely used turbulence models in industrial applications are based on Reynolds-averaged Navier–Stokes first-order closures. The first category places the first calculation node outside the viscous sub-layer, and by linking boundary conditions at the wall to points in the inner part of the domain by 'wall laws' (see Reference [1] for the theory and Reference [2] as an example of implementation in a code), these models avoid modelling vanishing effects and extreme anisotropy of near-wall turbulence and most of all, the numerical difficulties due to sharp variations of the variables near the wall. Thus, they lead to faster convergence and allow to use coarse meshes. But they are valid only for high-Reynolds number (HRN) flows, are based on strongly limiting assumptions and hence do not take into account sufficient phenomena in the near-wall area for many complex flows (streamline curvatures [3], external forces such as adverse pressure gradients or buoyancy, stagnation or separation points [4], unsteadiness, heat or mass transfers). The alternative is to solve the equations up to the wall,

*Correspondence to: V. Boyer, EDF, MFTT, 6 quai Watier, B.P. 49, 78400 Chatou Cedex, France.
†E-mail: vincent.boyer@edf.fr

Contract/grant sponsor: Electricité de France R&D (MFTT).

Received May 2001
Revised October 2001

with natural boundary conditions. This approach, known as low-Reynolds number (LRN) formulation (first developed by Jones and Launder [5], widely reviewed in Reference [6]), provides better results, but necessitates grids so fine that they are too demanding for super computer memories in many industrial applications. Moreover, even if unstructured or non-conforming grids allow to consider local refinements only in selected parts of the geometry, no existing method allows to combine local mesh refinement and LRN modelling in critical regions of an otherwise generally HRN calculation for most of the geometry, i.e. there is no numerical transition procedure between the HRN and LRN areas of the flow.

The model proposed in the present work synthesizes both the HRN and LRN formulations. In the HRN areas, coarse cells can be used, and in the LRN parts, cells size could go down to $y^+ = 1$ (typical value of the distance to the wall in 'wall units' y^+ in standard LRN models), whereas it is restricted to $y^+ > 30$ in the HRN formulation. Still based on the concept of wall functions, this model is as general as possible, since standard equilibrium assumptions are not made during the elaboration of the new laws of the wall. Therefore, one can anticipate that it should produce improved results for a wide range of flows. The algorithm, integrating the finite volume-finite element method with unstructured grids (see Reference [7]), is an extension of the standard laws of the wall, also inspired from the two-layer models [8]. But it is based on the use of refined shape functions and most of all with independent scaling factors for each of the physical variables in the near-wall control volumes. Finally, it relies on an energetic approach as the wall functions are determined through energy conservation equations in the near-wall control volumes.

2. DESCRIPTION OF THE MODEL

2.1. Discretization of the domain

The domain is divided into two layers: the near-wall layer and the outer layer of the flow. In the latter, one considers a standard LRN model with a cell-centred finite volume discretization. Calculations have been performed using the well-known Launder and Sharma model [9] used in the inner layer, but more sophisticated models can also be implemented (non-linear eddy-viscosity models, differential Reynolds-stress models, V2F [10], etc.). In the near-wall cells of the mesh, U, k and ε are described by the non-dimensional shape functions $F_u(y^+), F_k(y^+), F_\varepsilon(y^+)$ multiplied by scaling factors introduced in such a way that they are analogous to the usual friction velocity u_*:

$$\begin{aligned} U(y) &= s_u F_u(y^+) \\ k(y) &= s_k^2 F_k(y^+) \\ \varepsilon(y) &= \frac{s_\varepsilon^4}{\nu} F_\varepsilon(y^+) \\ y^+ &= \frac{s_y}{\nu} y \end{aligned} \tag{1}$$

The shape functions are complex enough to include the dependence of the variables (especially for k) on the turbulent Reynolds number and mimic the asymptotic behaviour of the

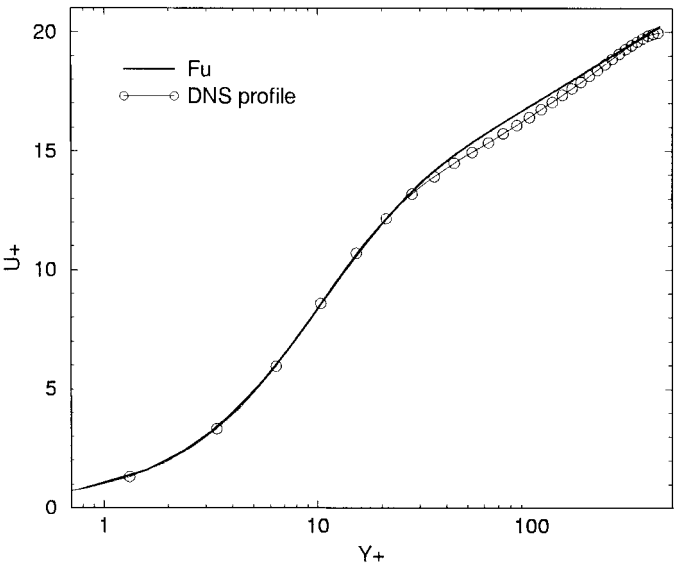

Figure 1. Shape function for the velocity.

flow at the wall. Thus, for the velocity, the well-known Reichard law

$$F_u(y^+) = \frac{1}{0.41}\ln(1 + 0.41y^+) + 7.8\left(1. - e^{-y^+/11} - \frac{y^+}{11}e^{-y^+/3}\right) \tag{2}$$

shown in Figure 1, is used.

The profile for the turbulent kinetic energy (which depends on the turbulent Reynolds number Re) is obtained by fitting direct numerical simulation (DNS) results for a closed-channel flow. It reads thus:

$$F_k(y^+) = \left[0.057 + 0.05\sqrt{\frac{Re}{1600}}\right] y^{+^2} e^{-y^+/7.3} + 4.6[1 - e^{-y^+/20}]\frac{1}{4y^+/Re + 1}[1 - e^{-(y^+/3)^2}] \tag{3}$$

Several profiles for different Reynolds numbers are drawn in Figure 2.

F_ε is also an analytical function fitting DNS results, which reproduces the theoretical $1/\kappa y$ behaviour in the logarithmic zone (see Figure 3):

$$F_\varepsilon(y^+) = \frac{1}{\kappa(y^{+4} + 15^4)^{1/4}} \tag{4}$$

2.2. Algorithm of resolution

The outer Navier–Stokes solver provides values of the variables in the outer layer, which can then be interpolated to obtain the values of the turbulent kinetic energy $k(h)$, the velocity $U(h)$, and the dissipation rate $\varepsilon(h)$ at the separation between the two layers. In the near-wall layer, instead of solving the usual equations (momentum equation and k-equation),

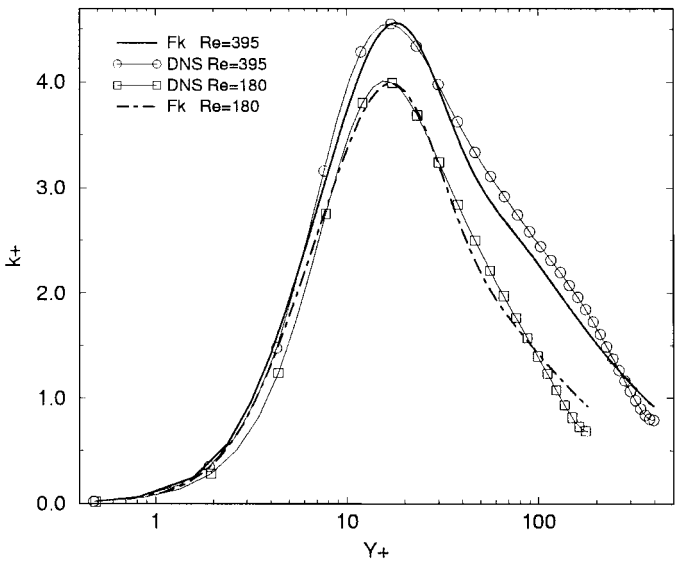

Figure 2. Shape function for the turbulent kinetic energy.

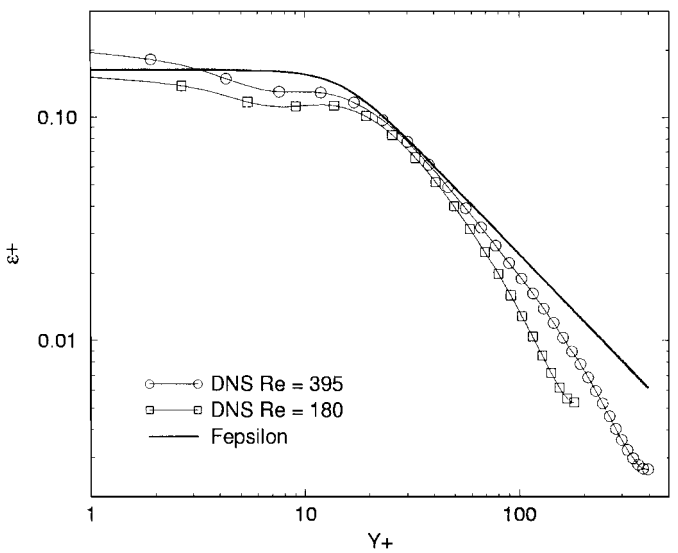

Figure 3. Shape function for the dissipation rate.

energy conservation equations are written, consisting of the mean flow energy balance and the turbulent kinetic energy balance in the first cells. These balances are obtained without any assumptions by integration over the first control volume of the momentum equation multiplied

by the velocity, which leads, one-dimensionally to

$$\left[-\overline{uv}U + \nu\frac{\partial U}{\partial y}U\right]_{(h)} - \int_0^h -\overline{uv}\frac{\partial U}{\partial y}\,\mathrm{d}y - \nu\int_0^h \frac{\partial U}{\partial y}^2\,\mathrm{d}y + \gamma_{\text{ext}}\int_0^h U\,\mathrm{d}y = \frac{\partial}{\partial t}\int_0^h \frac{U^2}{2}\,\mathrm{d}y \tag{5}$$

while integration of the k-equation leads to

$$\int_0^h -\overline{uv}\frac{\partial U}{\partial y}\,\mathrm{d}y - \int_0^h \varepsilon\,\mathrm{d}y + \left[(\nu+\nu_t)\frac{\partial k}{\partial y}\right]_{(h)} = \frac{\partial}{\partial t}\int_0^h k\,\mathrm{d}y \tag{6}$$

h being the size of the first cell and γ_{ext} the external forces (including pressure gradient, buoyancy, rotation effects, etc.). The closure is made with a linear eddy-viscosity model

$$-\overline{uv} = \nu_{\text{t}}\frac{\partial U}{\partial y} \tag{7}$$

where the eddy viscosity is defined through another shape function

$$\begin{aligned} \nu_{\text{t}} &= f_\mu(y^+)\,y\,k^{1/2} \\ f_\mu(y^+) &= C_\mu^{te}(1-\mathrm{e}^{-y^+/A_\mu})^2 \end{aligned} \tag{8}$$

Profiles (1) are then cast into the energy balances (5) and (6) for each iteration. With equations (1) written at point h, using the values $U(h)$ and $\varepsilon(h)$, this leads to a set of four algebraic equations that one can solve to determine the scaling factors. Finally, boundary conditions to be applied at the separation for the next iteration of the outer solver are expressed in terms of scaling factors and shape functions, which are then known for every variable. Neumann conditions (flux conditions) are applied for the velocity and the dissipation rate, i.e.

$$\left.\frac{\partial U}{\partial y}\right|_{y=h} = s_u\frac{s_y}{\nu}F_u'(h^+) \tag{9}$$

and

$$\left.\frac{\partial \varepsilon}{\partial y}\right|_{y=h} = \frac{s_\varepsilon^4 s_y}{\nu^2}F_\varepsilon'(h^+) \tag{10}$$

while a Dirichlet condition is used for the turbulent energy, easily expressed as

$$k(h) = s_{\text{k}}^2 F_k(h^+) \tag{11}$$

Remark
Although one prefers writing boundary conditions as fluxes, especially in an FV formalism, fixing the value of at least one of the variable somewhere in the mesh through this Dirichlet condition is necessary to ensure consistency (see Reference [2]).

2.3. Determination of the scaling factors

From $U(h)$ and $\varepsilon(h)$ values of the velocity and the dissipation rate at the separation provided by the n^{th} inner solver iteration, the algorithm used for searching the scaling factors used can

be described as follows:

- Determine s_y^{n+1} as the solution of the implicit relation through the fix-point method

$$s_y = \frac{U(h)}{F_u(hs_y/v)} \tag{12}$$

  Then one defines

$$h^+ = \frac{hs_y^{n+1}}{v} \tag{13}$$

- Using this new value h^+, initialize s_ε and s_u by

$$\begin{aligned} s_\varepsilon &= \frac{\varepsilon(h)}{F_\varepsilon(h^+)} \\ s_u &= s_y^{n+1} \end{aligned} \tag{14}$$

- Determine s_{k}^{n+1} as the unique positive root of the following polynomial, resulting from the kinetic energy budget

$$A(h^+)s_{\mathrm{k}}^2 + B(h^+)s_{\mathrm{k}} + C(h^+) = 0$$

$$\begin{aligned} A(h^+) &= s_y^{n+1} f_\mu(h^+)h^+\sqrt{F_k(h^+)}F_k'(h^+) - \int_0^{h^+} F_\varepsilon(y^+)\,\mathrm{d}y^+ \\ B(h^+) &= (s_y^{n+1})^2 F_k'(h^+) \\ C(h^+) &= s_u^2 s_y^{n+1} \int_0^{h^+} f_\mu(y^+)y^+\sqrt{F_k(y^+)}F_u'^2(y^+)\,\mathrm{d}y^+ \end{aligned} \tag{15}$$

  It is obtained after the introduction of the scaling factors s_u, s_ε and s_y coming from the former operations, and the shape functions (2)–(4) in the turbulent energy conservation equation (6), assuming that the flow is steady.
- In the same way, determine s_u^{n+1} as the solution of

$$D(h^+)s_u + E(h^+) = 0$$

$$\begin{aligned} D(h^+) &= s_y^{n+1}F_u(h^+)F_u'(h^+)[f_\mu(h^+)h^+ s_{\mathrm{k}}^{n+1}\sqrt{F_k(h^+)} + s_y^{n+1}] \\ &\quad - s_y^{n+1}\int_0^{h^+}[f_\mu(y^+)y^+ s_{\mathrm{k}}^{n+1}\sqrt{F_k(y^+)} + s_y^{n+1}]F_u'^2(y^+)\,\mathrm{d}y^+ \\ E(h^+) &= \gamma_{\mathrm{ext}} v \int_0^{h^+} F_u(y^+)\,\mathrm{d}y^+ \end{aligned} \tag{16}$$

  deriving from the momentum balance (5).

- Apply the relation

$$s_\varepsilon^{n+1} = \sqrt[1/4]{(s_\mathrm{k}^{n+1})^3 s_y^{n+1}} \tag{17}$$

  deriving from the Kolmogorov analysis to obtain the last scaling.
- Write $s_y = s_y^{n+1}$, $s_u = s_u^{n+1}$, $s_\mathrm{k} = s_\mathrm{k}^{n+1}$, and $s_\varepsilon = s_\varepsilon^{n+1}$.
- Finally, apply boundary conditions through relations (9)–(11)

Remark
In opposition to standard wall functions, s_y is not presumed identical to s_k since Kolmogorov scaling would require that it also depends on s_ε. Actually, the new approach is an extension of the usual wall functions' features where only two different scalings are used (in the best case) with very simple shape functions (if not simplistic). Indeed, a parallel between the newly proposed approach and the classical 'two velocity scales' leads to expressing the latter as

$$s_u = u_*, \quad s_\mathrm{k} = s_y = u_k, \quad s_e^3 = u_k u_k u_*$$
$$F_u(y^+) = \frac{1}{\kappa}\ln(y^+) + C$$
$$F_k(y^+) = (C_\mu)^{-1/2}$$
$$F_\varepsilon(y^+) = \frac{1}{\kappa y^+}$$

Furthermore, the model does not rely on the standard equilibrium assumption (production equals dissipation) and takes into account the influence of the external forces γ_ext.

3. RESULTS AND PERFORMANCES

The model is at first tested in a 1D steady closed-channel flow at several Reynolds numbers $Re = eu_*/\nu$ (e being the half-width of the channel). The LRN model chosen for the inner layer of the domain is the well-known Launder and Sharma model [4] for its simplicity. The cell-centred finite volume method is applied only to the outer part of the flow, as the near-wall layer is totally described by the scaling factors and the shape functions. Then the mesh starts at distance h from the wall, up to distance e and contains N control volumes (of arbitrary sizes). One has to keep in mind that values calculated at the centre of the cells represent averaged values over the cells. At the boundary $y = h$, values needed by the algorithm for the determination of the scalings (e.g. $U(h), \varepsilon(h), \ldots$) are interpolated from the mean values in the first cells of the mesh and fluxes between the two layers. The boundary conditions needed in the finite volume formulation, are expressed directly by (9) and (10) or reconstructed from (11). The equations of the turbulent variables are coupled to increase the stability of the resolution. The matrix deriving from the discretization is

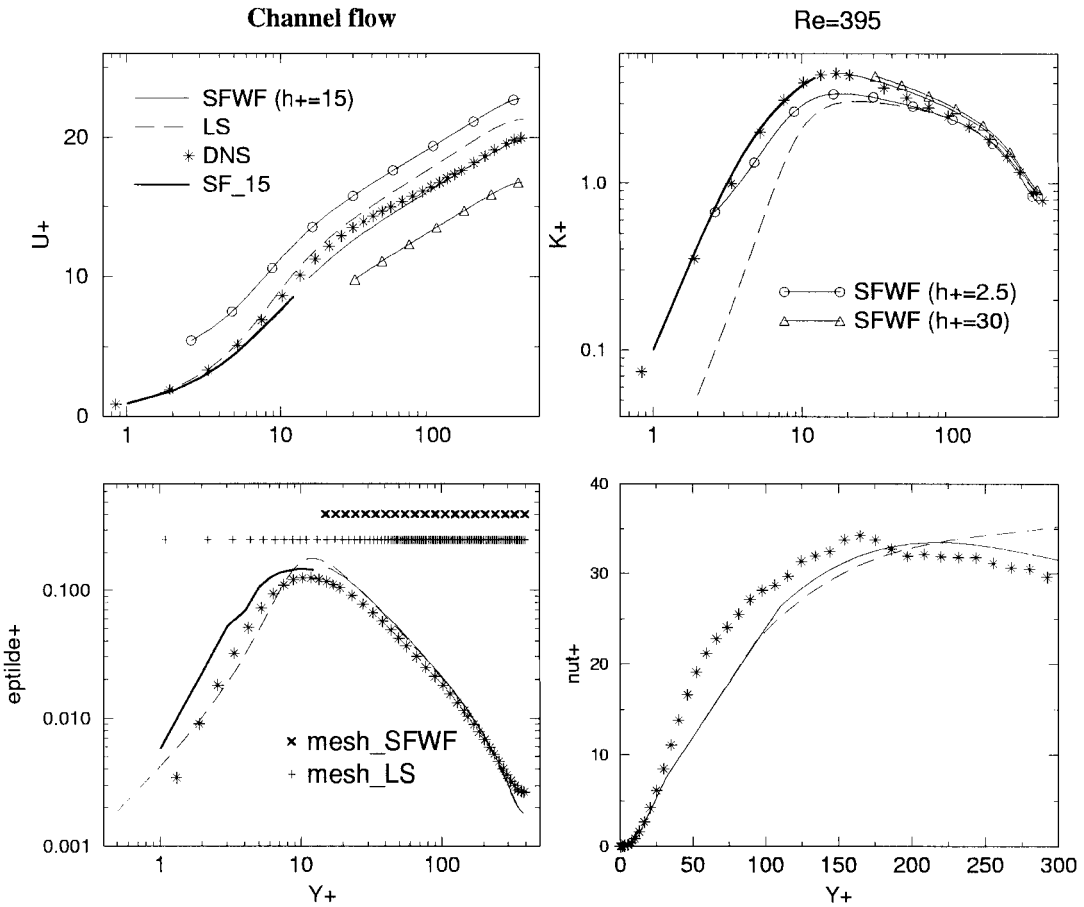

Figure 4. Closed channel-flow results at turbulent Reynolds $Re = 395$.

solved by a BiCG-Stab algorithm (because of the coupling, the matrix to be inverted is not symmetrical).

Results obtained with the new shape function–wall function approach (denoted SFWF) are compared in more Figure 4 with direct numerical simulation (or DNS) data and Launder and Sharma (or LS) results in the case of $Re = 395$ (low-Reynolds number flow). This is not limitative, the results being similar to $Re = 180$ and 2000. Most of the results shown correspond to a first cell size $h^+ = 15$ (SFWF ($h+ = 15$) in the legend), because this value is the most difficult to deal with (as it corresponds to the peaks in k and ε) and corresponds to the cell sizes leading to poor results with the HRN formulation. Though, a wide range of sizes have been tested, from $h^+ = 2.5$ to 100, to ensure that the new approach provides good results, for any value of h. As the first cell is not taken into account in the resolution of the inner solver, shape functions multiplied by the scalings provided by the calculation have been added to the budgets (see *SF*_15).

Remark
The results presented Figure 4 are non-dimensional, which means they are normalized as in the following:

$$\begin{aligned} U^+ &= \frac{U}{s_u} \\ k^+ &= \frac{k}{s_k^2} \\ \tilde{\varepsilon}^+ &= \frac{\tilde{\varepsilon}^v}{s_{\tilde{\varepsilon}}^3} \\ v_t^+ &= \frac{v_t}{v} \end{aligned} \tag{18}$$

Note that in order to simplify the comparison between SFWF and LS results, $\tilde{\varepsilon}$ has been used instead of ε. Both can be related by the relation

$$\tilde{\varepsilon} = \varepsilon - 2v\left(\frac{\partial\sqrt{k}}{\partial y}\right)^2 \tag{19}$$

The SFWF method provides much better results than LS, particularly concerning the prediction of the turbulent energy k peak (see k-budget), the conservation of the flow rate (overestimated by LS) and the prediction of the turbulent viscosity in the central part of the channel. Still this is an obvious consequence of the proper tuning of the shape functions on the DNS data, and the main achievement here is that results concerning U, $\tilde{\varepsilon}$, and v_t are completely independent of the chosen h. Velocity profiles SFWF ($h+=2.5$) and SFWF ($h+=30$) (for $h_+=2.5$ and 30) have been added to the U-budget They have been offset by a constant (± 3) for visibility, but they are strictly identical to SFWF ($h+=15$). More sensitivity to h is found for k, probably due to the Dirichlet condition (11) leading to the dependence of the solution on the accuracy of F_k in describing the true k-profile. Nevertheless, for any value of h, the k-budget is bounded by the curves SFWF ($h+=2.5$) and SFWF ($h+=30$), and thus always shows a better agreement with the DNS data than in the LS case.

In addition, the new algorithm is endowed with great stability and very fast convergence. The LS model needs grids five times finer than SFWF to reach spatial convergence. Moreover, the maximum time step allowed by SFWF is from 5 to 30 times greater than the one in LS calculation, i.e. inversely proportional to the first cell size as can be expected from physical arguments, which implies large time and memory savings for industrial calculations. For example, when $h^+=30$, SFWF only needs 250 iterations, to converge, versus 2000 for the LS calculation. To illustrate meshing savings, those used for the H_15 and LS calculations have been added to $\tilde{\varepsilon}^+$-budget (referring to the dissipation rate $\tilde{\varepsilon}$ used in the Launder and Sharma model, normalized).

4. CONCLUSION

A new numerical approach based on intensive use of complex shape functions for all the variables in the first cell of the domain is proposed, in order to reach the challenging aim of

modelling the wall behaviour of the flow with the same accuracy as an LRN, whatever the size of the near-wall cell. This approach, named in the present work SFWF (for shape function–wall function) is as general as possible as no restrictive equilibrium assumption is made, and the formulation is universal (code independent). The results obtained in the simple case of a fully-developed channel flow are very encouraging, concerning both the accuracy and the numerical stability, even if the model has not been tested yet in more complex configurations (3D, buoyancy, adverse pressure gradients, etc.). Moreover, it is very promising for industrial applications, as it leads to fast convergence and allows the use of coarse meshes.

NOMENCLATURE

y	distance to the wall
h	size of the near-wall cell
y^+, h^+	non-dimensional distances
U	velocity
k	turbulent kinetic energy
ε	dissipation rate
$\tilde{\varepsilon}$	dissipation rate in the Launder and Sharma model
u_*	friction velocity
s_y	scaling factor for the distance to the wall
s_u	scaling factor for the velocity
s_k	scaling factor for the turbulent kinetic energy
s_ε	scaling factor for the dissipation rate
ν	molecular viscosity
ν_t	turbulent viscosity
$-\overline{uv}$	shear stress
t	time
f_μ	shape function for the turbulent viscosity
A_μ, C_μ^{te}	constants used to define f_μ
γ_ext	external forces
e	half-width of the channel
$n+1$	refers to the current time iteration

ACKNOWLEDGEMENTS

The first author would like to thank Electricité de France R&D (MFTT) for financial support throughout his MPhil at UMIST.

REFERENCES

1. Viollet PL, Chabard JP, Esposito P, Laurence D. *Mécanique des Fluides Appliquée*. Presse des Ponts et Chaussées, 1999.
2. Boucker M, Mattéi JD. Proposition de modification des conditions aux limites de paroi turbulente pour le Solveur Commun dans le cadre du modèle $k-\varepsilon$ standard. *Note interne EDF*, *HI*-81/00/0/9/A, 2000.
3. Launder BE, Priddin CH, Sharma BI. The calculation of boundary layers on spinning and curved surfaces. *Journal of Fluids Engineering* 1977; 231–239.

4. Craft TJ, Graham LJW, Launder BE. Impinging jet studies for turbulence model assessment—II: an examination of the performance of four turbulence models. *International Journal of Heat and Mass Transfer* 1993; **36**: 2685–2697.
5. Jones WP, Launder BE. The prediction of laminarization with a two-equations model of turbulence. *International Journal of Heat and Mass Transfer* 1972; **15**:301–314.
6. Patel VC, Scheuerer RW. Turbulence models for near-wall and low-Reynolds numbers flows: a review. *AIAA Journal* 1985; **23**(9):1308–1319.
7. Ferziger JH, Peric M. *Computational Methods for Fluids Dynamics* (2nd edn). Springer: Berlin, 1999.
8. Rodi W, Mansour NN, Michelassi V. One-equation near-wall turbulence modeling with the aid of direct simulation data. *SFB 210/T/93*, 1993.
9. Launder BE, Sharma BI. Application of the energy-dissipation model of turbulence to the calculation of flow near a spinning disc. *Letters in Heat Mass Transfer* 1974; **1**:131–138.
10. Durbin PA. Near-wall turbulence closure modeling without damping functions. *Theoretical and Computational Fluid Dynamics* 1991; **3**:1–13.

